JOURNAL OF APPLIED ELECTROCHEMISTRY **28** (1998) 579–587

The influence of fluid flow on levelling performance

Q. CHEN*, V. MODI*, A. C. WEST‡

*Department of Mechanical Engineering, and ‡Department of Chemical Engineering Materials Science and Mining Engineering, Columbia University, New York, NY 10027, USA

Received 10 February 1997; revised 1 August 1997

The influence of fluid flow on electrode-shape change that results from electrodeposition in the presence of a model, levelling agent is simulated and discussed. The treatment is more rigorous than past studies in that flow and concentration fields are recalculated as the electrode shape changes. It is shown that uncertainties due to approximate treatments of fluid flow may be as significant as existing discrepancies between experiment and theory. A numerical algorithm necessary to minimize errors associated with automatic grid generation is discussed.

Keywords: *fluid flow*, *levelling*, *shape change*

List of symbols

a_i	distance of line segment connecting points P_{i-1} and P_i (see Fig. 4(c))
b_i	distance of line segment connecting points L_i and R_i (see Fig. 4(c))
c_a	dimensionless concentration of inhibitor
c_{bulk}	bluk concentration of inhibitor (mol m^{-3})
D	diffusion coefficient (m^2 s^{-1})
e	parameter used for evolution of boundary shape
F	Faraday's constant (96 487 C mol^{-1})
G_i	distance from intersection of two neighbour bisectors of electrode surface
g_i	dimensionless growth height
H	height of the simulation domain
h_0	the depth of the semicircular trench, also the characteristic length scale (m)
i	current density (A m^{-2})
i^*	dimensionless current density
i_{no}	current density without the presence of inhibitor (A m^{-2})
k_a	kinetic parameter relating inhibition to levelling-agent flux (mol A^{-1} s^{-1})
L	length of the simulation domain
L_a	dimensionless parameter ($= c_{bulk}D/k_a i_{no}$)
L_0	dimensionless distance shown in Fig. 1
N_a	flux of inhibitor to electrode (mol m^{-2} s^{-1})
n	normal direction of the boundary
n_m	number of electrons transferred during deposition
Re	Reynolds number $\left(Re = S_x h_0^2/\nu\right)$
Sc	Schmidt number (ν/D)
S_x	shear at inlet of simulation domain
SS	the south boundary shape in the process of the boundary movement
S_{avg}	average distance of two neighbouring points on south wall (represented by SS)
x_0	the x coordinate of the starting point of the electrode
TT	the south boundary shape generated by GridPro in solving the concentration field
U	dimensionless velocity vector
Δt	dimensionless time step
w	evaluated at a solid wall

Greek symbols

δ	trench depth (see Fig. 8)
ν	kinematic viscosity (m^2 s^{-1})
ψ	dimensionless stream function
ρ_m	density of the metal (mol m^{-3})
ω	dimensionless vorticity
γ	underrelaxation factor for vorticity at solid wall

1. Introduction

Additives are often included in electroplating baths for modification of the deposit structure. Such additives can also adversely influence deposit purity. A lack of a firm understanding of bath additives can be troublesome for high-technology applications found in the electronics industry, where quality control is vital. One type of additive, known as levelling agents, is discussed here.

In common theories, levelling agents are assumed to inhibit deposition by an amount proportional to their flux to the electrode [1]. Levelling is therefore assumed to occur because the additive flux and thus inhibition is greater on the 'hills' of a rough surface than the 'valleys'. Tobias and coworkers have reviewed thoroughly previous studies of levelling agents [2, 3]. They have also performed shape-change simulations and compared their numerical results to the classical, experimental work [4, 5] on the role of coumarin in nickel deposition.

More recently, Madore *et al.* [6, 7] presented an extensive experimental and numerical study of the influence of coumarin on levelling during nickel de-

0021-891X

position. Even though their work is the most complete to date, discrepancy still exists between the calculated and the experimental levelling powers. Part of the discrepancy may be due to the approximate manner (by necessity because of the electrode and cell design) in which fluid flow is treated in their analysis.

Progress in the development of predictive models for levelling has been difficult because of the need to understand the mass-transfer (and thus fluid-flow) phenomena as well as the chemical and electrochemical interactions between the levelling agent and the electrode, reactants, and/or possible reaction intermediates [8]. Fluid flow has been treated previously by assuming a stagnant diffusion layer, whose thickness depends on flow rate.

Jordan and Tobias [10] addressed issues concerning the approximate treatments of flow but only calculate flow fields for the initial electrode shape. A more rigorous analysis of flow requires that the flow be recalculated as the electrode shape changes. Such problems may be difficult because of the need to regenerate the discretization grid at every, or at least several, time steps. In fact, the grid-generation step is found in the present study to be the major source of numerical error, unless adequate procedures are followed.

The purpose of the present communication is to show the influence of fluid flow on numerical simulations of a previously proposed model [3]. Polarization curves and impedance measurements indicate that the model is valid when the ratio of the nickel to coumarin fluxes at the electrode are large [9]. Results indicate that changes in levelling performance with flow conditions may be significant. Jordan and Tobias [10] conclude that a stagnant-diffusion layer approximation for the fluid flow is satisfactory. The results presented here are largely in agreement with this statement but also indicate that flow effects can introduce discrepancies between simulations and experiments, depending on how data are analysed. Implications for experimental design and for all elucidation of the details of the levelling mechanism are discussed.

2. Theory

2.1. *Levelling model*

We use the model of Jordan and Tobias [3]. The development of the equations and the physical justification can be found in their paper. In summary, the following assumptions are used: (i) the flux of levelling agent is mass-transfer controlled; (ii) the electrode shape change is sufficiently slow that the concentration fields at any instant in time are given by a steady-state analysis (for the appropriate electrode shape); (iii) the inhibitors act by blocking the electrode surface, reducing the electrode surface area available for electrodeposition.

According to Jordan and Tobias [3], the metal deposition rate is given by

$$i = i_{\mathrm{no}} - \frac{1}{k_{\mathrm{a}}} N_{\mathrm{a}} \tag{1}$$

where i_{no} is the current density that would be obtained in the absence of inhibitor, k_{a} is a kinetic parameter, and N_{a} is the flux of inhibitor to the electrode given by

$$N_{\mathrm{a}} = c_{\mathrm{bulk}} D \left.\frac{\partial c_{\mathrm{a}}}{\partial n}\right|_{\mathrm{w}} \tag{2}$$

where the c_{bluk} is the bulk concentration of the inhibitor, c_{a} is the dimensionless concentration of inhibitor and n is the direction normal to the boundary.

We assume that the Wagner number is sufficiently large that the current distribution would be uniform in the absence of levelling agent; that is, i_{no} is not a function of position. Substitution of Equation 2 into Equation 1 gives

$$i^* = 1 - L_{\mathrm{a}} \left.\frac{\partial c_{\mathrm{a}}}{\partial n}\right|_{\mathrm{w}} \tag{3}$$

Here, $i^* = i/i_{\mathrm{no}}$ is the dimensionless current density and L_{a} is a parameter defined by

$$L_{\mathrm{a}} = \frac{c_{\mathrm{bulk}} D}{k_{\mathrm{a}} i_{\mathrm{no}}} \tag{4}$$

The average amount of inhibition is given by $L_{\mathrm{a}}(\partial c_{\mathrm{a}}/\partial n)|_{\mathrm{avg}}$. For a sufficiently large flux to the wall, Equation 3 predicts a negative dimensionless current, corresponding to metal dissolution. Dissolution does not occur for the cathodic overpotentials used in most levelling studies. Instead, a large flux of levelling agent will correspond to a nearly zero current density. In the present simulations, we have set all negative i^* to zero. Such an approximation is not too unrealistic, when compared to polarization curves obtained for nickel deposition in the presence of coumarin [9].

After solving for the concentration field, the current density is obtained from Equation 3. The boundary is then moved according to a dimensionless form of Faraday's law:

$$\Delta h = -i^* \Delta t \tag{5}$$

In Equation 5, $\Delta t = i\Delta t'/(n_{\mathrm{m}} F h_0 \rho_{\mathrm{m}})$ is a dimensionless time. In the numerical method, Δt is set to be sufficiently small to obtain accuracy in the boundary movement.

2.2. *Initial geometry and flow*

Simulations have been performed for both triangular and semicircular trenches. Results are only presented for the semicircular case because, as Madore *et al.* [6, 7] discuss, this geometry allows for a more careful distinction between true and geometric levelling.

A flow with uniform shear S_x from the west as shown in Fig. 1 is assumed. In the presence of a shear flow, the diffusion layer thickness is a function of position. To eliminate ambiguities associated with

setting the thickness in the vicinity of the trench, we assume that the electrode, upon which additive is consumed, begins at a dimensionless position $L_0 - x_0$ upstream of the centre of the trench. All lengths are made dimensionless with respect to the initial trench height h_0. The actual values used in the simulations are $L = 26,\ H = 4,\ L_0 = 19$, and $x_0 = 1$, except when $Re \leqslant 0.01$, where the concentration boundary layer thickness is large. For $Re = 0.01$, the values $H = 6$ and $x_0 = 2$ were used. Computer experiments show that simulation results do not change with larger values of L or H. This indicates that the simulations on a finite domain adequately approximate the semi-infinite domain case.

At the intersections of the semicircular trench with the flat boundary, small circular arcs are used for the initial electrode contours to avoid sharp corners, which adversely affect the boundary movement algorithm. The dimensionless radius of the arc is 0.1 and it is tangent to both the flat surface and the semicircular trench.

In the present study, the Schmidt number is chosen to be $Sc = \nu/D = 1000$, typical for electrochemical systems. The Reynolds number is given by

$$Re = \frac{S_x h_0^2}{\nu} \tag{6}$$

3. Numerical method

3.1. *Fluid flow and concentration solution scheme*

The spatial distribution of the flux of additive depends on the fluid flow. Here, the flow is determined from the stream-function vorticity formulation of the steady Navier–Stokes equations using a semidirect method suggested by Roache [11]. In the stream-function/vorticity formulation, the Navier–Stokes equations reduce to

$$\nabla^2 \psi = -\omega \tag{7}$$

$$Re\left(\frac{\partial}{\partial x}(u_x \omega) + \frac{\partial}{\partial y}(u_y \omega)\right) = \nabla^2 \omega \tag{8}$$

in nondimensional form, with characteristic velocity and length scales $S_x h_0$ and h_0, where ψ is the stream function, which is related to flow velocities through $(\partial\psi/\partial y) = u_x$, $(\partial\psi/\partial x) = -u_y$ and ω is the vorticity defined as $\omega = (\partial u_y/\partial x) - (\partial u_x/\partial y)$. The concentration of levelling agent satisfies the convection–diffusion equation, which is of the same form as Equation 8. The concentration field is, therefore, obtained by the same algorithm as that for vorticity transport. A schematic diagram of the calculation domain is shown in Fig. 1. The boundary conditions are specified as follows. In the equations below, n and s are the normal and tangential directions to the boundary.

An assumption of uniform shear at the upstream boundary $x = 0$ corresponds to

$$\omega = -1 \qquad \psi = \tfrac{1}{2}y^2 \qquad c_a = 1 \tag{9}$$

At the flow exit $x = L$, outflow conditions are specified:

$$\frac{\partial \omega}{\partial n} = 0 \qquad \frac{\partial^2 \psi}{\partial n^2} = 0 \qquad \frac{\partial c_a}{\partial n} = 0 \tag{10}$$

In view of Equation 7, the second order boundary condition for ψ can be replaced with an ordinary differential equation at the flow exit [12]

$$\omega = -\frac{\mathrm{d}^2 \psi}{\mathrm{d}s^2} \tag{11}$$

The upper wall $y = H$ moves to the right with dimensionless speed H:

$$\omega = \frac{\partial^2 \psi}{\partial n^2} \qquad \psi = \tfrac{1}{2}H^2 \qquad c_a = 1 \tag{12}$$

No slip conditions are imposed at the electrode:

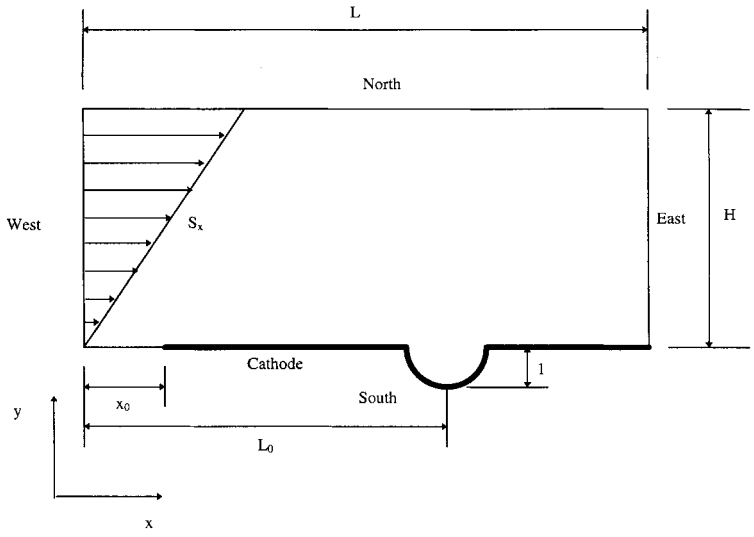

Fig. 1. Schematic diagram of the typical computational domain. A uniform shear flow enters the domain. The depth of the semicircular trench, h_0, is the characteristic length scale. All specified lengths are made dimensionless with respect to h_0.

$$\omega = -\frac{\partial^2 \psi}{\partial n^2} \qquad \psi = 0 \qquad c_a = 0 \qquad (13)$$

The boundary condition for vorticity at the solid wall is critical since it provides the coupling between the stream function and vorticity equations. A first order approximation to Equations 12 and 13 is used for the second derivative. Furthermore, an under-relaxation factor $\gamma = 0.02$ for the vorticity boundary condition at the wall is used. This under-relaxation takes the form of

$$\omega_w^{k+1} = \gamma \omega_w + (1-\gamma)\omega_w^k \qquad (14)$$

where ω_w denotes the vorticity at the wall obtained from Equation 12 or 13, ω_w^{k+1} is the vorticity at iteration level $k+1$, and ω_w^k is the vorticity at iteration level k.

3.2. *Code validation*

Two-dimensional, backward-facing step fluid flow was solved to validate the code. Particular attention was paid to how a nonorthogonal grid affects the prediction of the separation/reattachment point. The calculations were performed for cases of *Re* (based on the step height and mean velocity at the inlet of the channel) = 50, 75, 100, 125. The reattachment locations for various Reynolds numbers were in good agreement with experimental data of Armaly *et al.* [13] and simulation data of Cabuk *et al.* [4]. A solution of a mass-transfer problem for steady-state forced convection in laminar flow between two parallel plates was also obtained to verify the concentration-solution code. Results were in good agreement with the Leveque solution given by Newman [15].

3.3. *Grid generation and boundary movement*

After solving the fluid flow and concentration field, the inhibitor flux to the boundary is obtained. The current is then obtained from Equation 3. The following boundary movement algorithm was used:

(i) Initially, the south boundary is represented by (perhaps) 400 evenly distributed points, with straight line segments connecting the points. The distance between these points is S_{avg}. Every third point of the semicircular trench with an initial depth of h_0 is shown in Fig. 2.

(ii) Using the distribution of points on the electrode (shape A), a grid is generated using GridPro [16] for the solution of the flow and concentration fields. In order to generate a nearly orthogonal grid (desirable for the flow and concentration solvers), the grid generation software relocates the points to new positions (shape B), producing an undesirable distortion in the prescribed electrode shape. The initial mesh and an intermediate mesh so generated are shown in Fig. 3. The effect on the flow or concentration solutions of this distortion was found to be negligible. The cumulative effect of this distortion after several grid generation steps (note that each new flow solution requires a new grid), however, is no longer negligible compared to the boundary growth. Hence, after computing the flow/concentration solutions on shape B, the actual boundary movement is implemented on shape A. In this fashion the effect of boundary distortion due to the grid generation process is limited to the computation of the flow and concentration fields.

Fig. 2. In a typical simulation, the south boundary is represented by 400 evenly distributed points. Every third point is shown here.

(iii) The boundary representations as shown in Fig. 4(a) of the electrode for flow/concentration solution (shape TT) and the growth process (shape SS) are different. Consequently the current densities computed on shape TT must be transferred to shape SS. The algorithm for doing this is described below. Consider a point B with neighbours A and C on SS and point F with neighbours E and G on TT as shown in Fig. 4(a). For an arbitrary point B on SS, the closest point

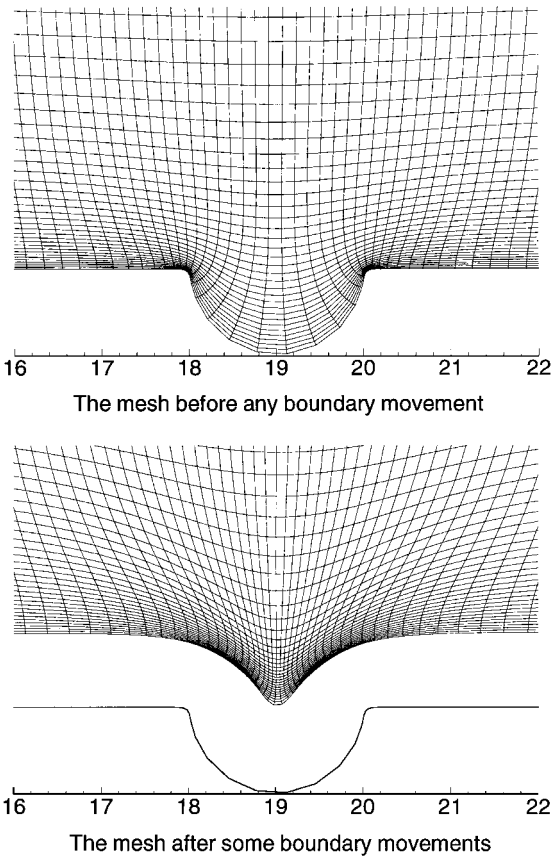

Fig. 3. Computational grids generated by GridPro for use in the fluid flow and concentration-field calculations. (a) Initial mesh. (b) An intermediate grid after shape change.

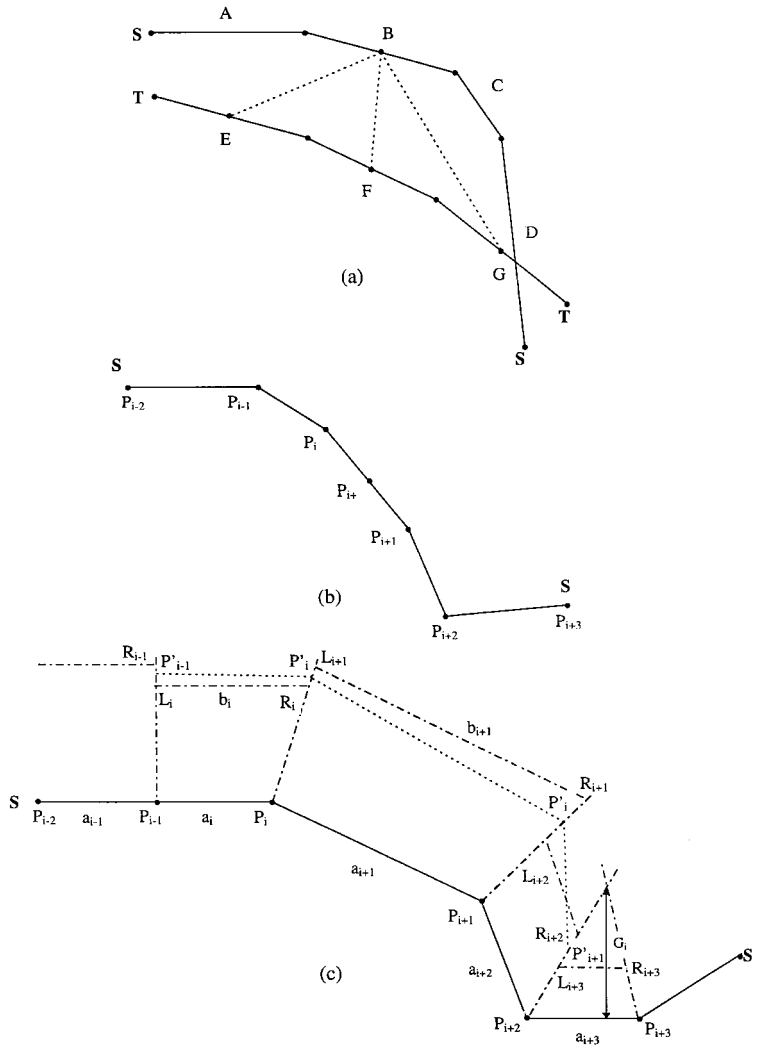

Fig. 4. (a) Schematic diagram to describe the process of transferring calculated current density from the computational grid to the grid used for shape change calculations. (b) Schematic diagram of the method to add and remove points in the process of boundary growth. (c) Schematic diagram of boundary growth that attempts to conserve quantity of new material deposited.

F on TT is found. The angles ∠FBE and ∠GBF are computed. If ∠FBE is greater (less) than ∠GBF, the current density $i^*|_B$ at B is determined as a weighted average of current densities at points F and E (F and G) on TT:

$$i^*|_B = \frac{1}{\overline{BF} + \overline{BE}} \left(i^*|_F \cdot \overline{BE} + i^*|_E \cdot \overline{BF} \right) \quad (15)$$

Using this algorithm, the current density on the entire shape TT is transferred to SS.

(iv) At the end of a growth step the points along SS are in general no longer evenly spaced. Successive steps may lead to points that are either too close or too far apart. An algorithm is used to add or remove points to correct this situation. Suppose that SS is described by points P_{i-1}, P_i, P_{i+1}, and P_{i+2}, shown on Fig. 4(b). If $\angle P_{i+2}P_{i+1}P_i$ is greater than 183° and the segment length $\overline{P_iP_{i+1}} > S_{avg}/3$, then an additional point P_{i+} is added between P_{i+1} and P_i. A segment length of $S_{avg}/3$ to trigger addition of points was found to adequately satisfy the needs of accuracy. The current densities i^* associated with the newly formed segments $P_{i+}P_{i+1}$ and P_iP_{i+} are taken to be the same as the current density associated with P_iP_{i+1}. A check is made on segment $P_{i+2}P_{i+1}$ next and so on. Wherever necessary, new points are added. To correct for points being too close, if a segment length $\overline{P_iP_{i+1}} < S_{avg}/6$, then either point P_i or P_{i+1} is removed. If P_i is removed, the current density associated with P_{i-1} and P_{i+1} is obtained by

$$i^*|_{P_{i-1}P_{i+1}} = \frac{1}{\overline{P_{i-1}P_i} + \overline{P_iP_{i+1}}} \cdot \cdot \left(i^*|_{P_{i-1}P_i} \cdot \overline{P_{i-1}P_i} + i^*|_{P_iP_{i+1}} \cdot \overline{P_iP_{i+1}} \right) \quad (16)$$

The point addition and removal processes are repeated recursively until no new points need to be added or removed. The addition and removal algorithms are always initiated at the lowest/highest points on the electrode in order to preserve the depth of the trench.

(v) The growth process implemented on shape SS must attempt to ensure that the quantity of new material deposited is conserved. Consider a point P_i on the initial shape SS with neighbours

P_{i-2}, P_{i-1}, P_{i+1}, and P_{i+2} as shown in Fig. 4(c) (see also Fig. 2). A bisector P_iP_i' of $\angle P_{i+1}P_iP_{i-1}$ is constructed. The lengths of line segments connecting P_{i-1} and P_i are denoted by a_i. The growth of a particular boundary segment is assumed to be confined to a region between two neighbouring bisectors. Points L_i and R_i on the bisectors on each side of a_i are located such that the line segment b_i connecting points L_i and R_i is parallel to a_i and the normal distance between a_i and b_i is the growth height g_i:

$$g_i = \frac{\Delta t_{\min} i^*|_i \, a_i}{(a_i + b_i)/2} \tag{17}$$

where $\Delta t_{\min}$ is determined from

$$\Delta t_{\min} = \frac{e}{\max(i^*|_i)} \tag{18}$$

where e must be less than 0.01 and less than $0.1(\min G_i)$. Here G_i is the normal distance from the intersection point of two neighbouring bisectors to the electrode surface as shown in Fig. 4(c). Thus ideally one would like the new growth shape to be given by line segments $\overline{L_{i-1}R_{i-1}}$, $\overline{L_iR_i}$, $\overline{L_{i+1}R_{i+1}}$ and so on. Since this surface is not continuous, a new surface shown by the dotted line in Fig. 4(c) is used. Thus each point P_i' defining the new shape is at the midpoint of the pair of points R_i and L_{i+1}.

(vi) Return to step (iv) and repeat the growth process until the product of $\max(i^*)$ and the cumulative step size $\sum \Delta t$ reaches 10% of the trench depth. Numerical experiments show that solving the fluid flow and concentration fields once after every additional deposition depth equal to 10% of the initial trench depth is adequate, since changes in current density are minor for changes in shape due to depositions less than this value.

(vii) Wherever an additional 10% deposition level is reached, the boundary points are evenly redistributed so that the distance between them is S_{avg}. This is a procedure similar to that of Madore *et al.* [6, 7] and Jordan and Tobias [3]. The redistribution starts from the lowest/highest points on the electrode. This eliminates any nonsmooth behaviour with length scales smaller than S_{avg} as well as ensures that the total number of points representing the boundary is stable. At this stage one returns to step (ii).

4. Results and discussion

It is important to correlate flow rate to the flux near the electrode 'scratch'. Figure 5 shows the average, initial dimensionless flux between the dimensionless positions $x = 16$ and 22 as a function of the Reynolds number. Of course, as deposition progresses, the average flux would change due to changes in the electrode shape. As a possible measure of the amount of change to be expected, the dashed line gives the average dimensionless flux obtained for a flat surface.

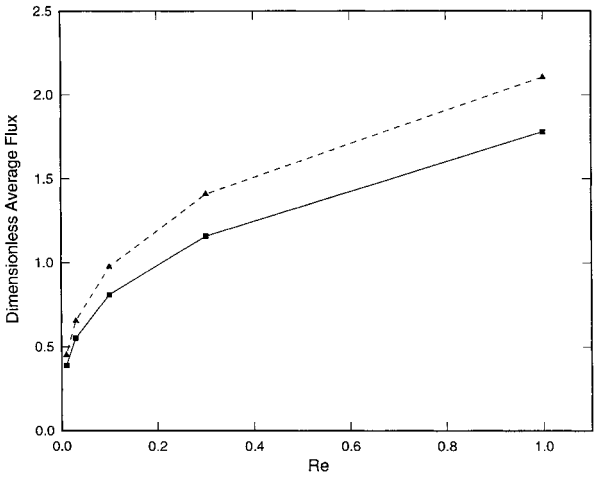

Fig. 5. Variation of dimensionless average flux of levelling agent to the electrode between $x = 16$ and $x = 22$ as a function of Reynolds number. The solid lines (——) are for the initial electrode shape (Fig. 1) and the dashed lines (– – – –) are for a flat electrode.

Figure 6 shows simulated electrode profiles for three Reynolds numbers and two values of inhibition constant L_a. As is most readily evident for the $Re = 1$ case, as L_a increases for a given flow rate, the amount of levelling increases. In the range of flow rates of the present study, for a given L_a, the levelling power increases with Re because the average flux increases. The increase in average flux leads to a larger variation in the current density (see Equation 3). The curves shown for the lower Re are nearly symmetric, while the $Re = 1$ results exhibit mild asymmetry due to the fluid flow.

Figure 7 shows a summary of some of the simulation results. In this Figure δ_{avg} is the average of the deposit thicknesses at $x = 16$ and 22 as shown in Fig. 8. The quantity δ_{avg} is plotted against the trench depth δ_t in Fig. 7. It is shown that the levelling rate, that is, the rate of decrease in δ_t, increases with L_a and with Re. For reference, the experimental results of Madore and Landolt [7] for geometric levelling are shown. The simulation of geometric levelling indicates that smoothing of the sharp corners near the trench has no significant effect on the numerical results. Furthermore, the ability to accurately simulate geometric levelling provided a means of determining a proper time step size.

Detailed simulation results for $Re = 0.1$ and $L_a = 0.2$ are shown in Fig. 9. In Fig. 9(a), the spatial distribution of the flux of levelling agent is shown for various dimensionless times. The electrode shape at each corresponding time is shown in Fig. 9(b). For the initial electrode shape, the flux distribution shows some asymmetry. This implies that the initial growth is larger at the leading edge of the trench. However, as the electrode shape changes, the flux distribution becomes nearly symmetric. This is perhaps a surprising result because $Pe = 100$, indicating that the flux of levelling agent is convectively dominated.

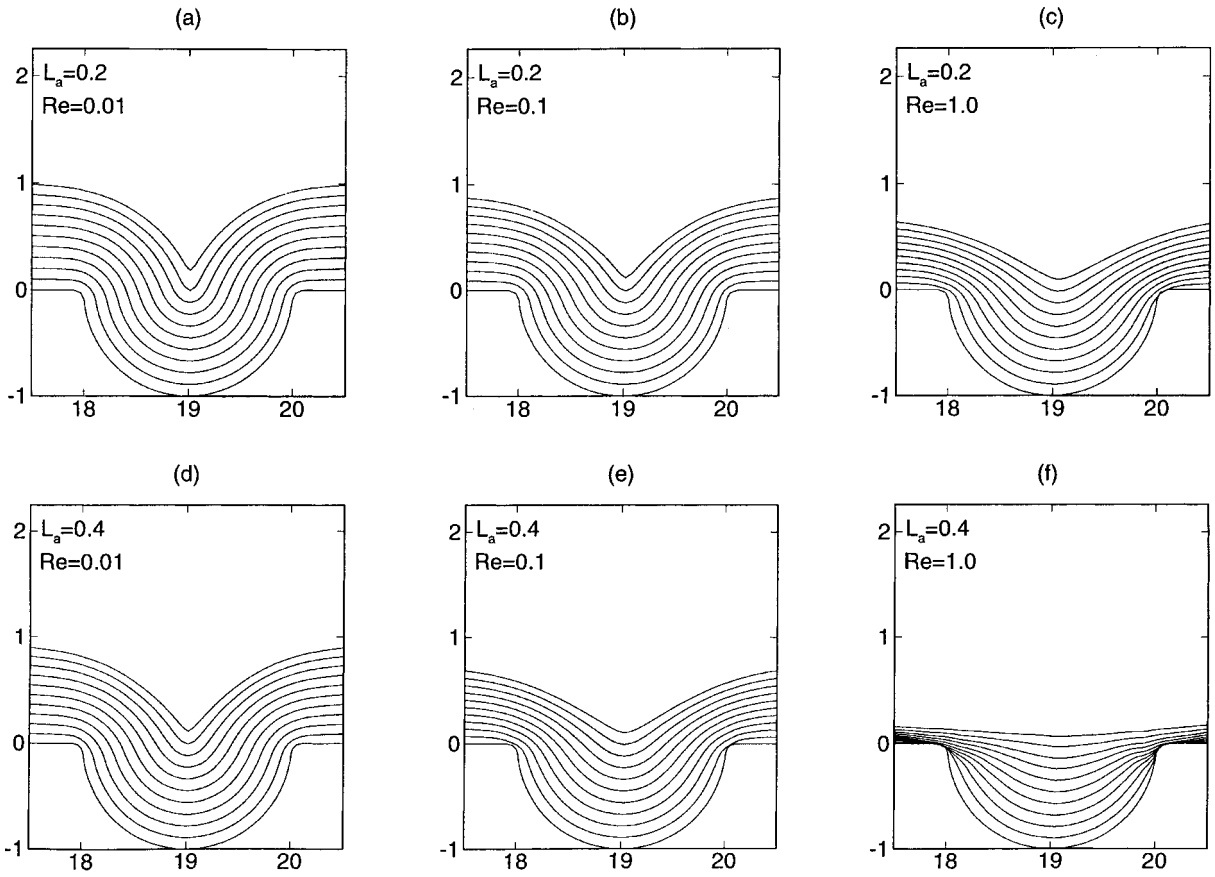

Fig. 6. Evolution of electrode shape for $L_a = 0.2$ and 0.4 and for Reynolds numbers of 0.01, 0.1 and 1.0.

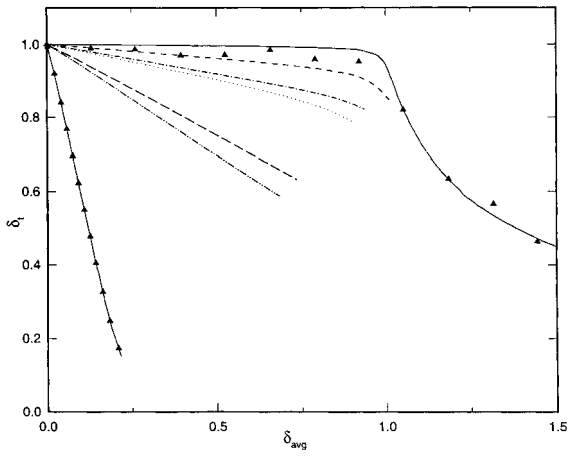

Fig. 7. Simulated depth of the trench as a function of the average deposit thickness δ_{avg}. Key: (———) geometric levelling; (- - - - -) $Re = 0.01, L_a = 0.2$; (·····) $Re = 0.01, L_a = 0.4$; (· · · · · · ·) $Re = 0.1$, $L_a = 0.2$; (– – – –) $Re = 0.1, L_a = 0.4$; (·····) $Re = 1.0$, $L_a = 0.2$; (—▲—) $Re = 1.0$, $L_a = 0.4$. Experimental data (▲) of Madore *et al.* [6, 7] for geometric levelling of semicircular trench are also shown.

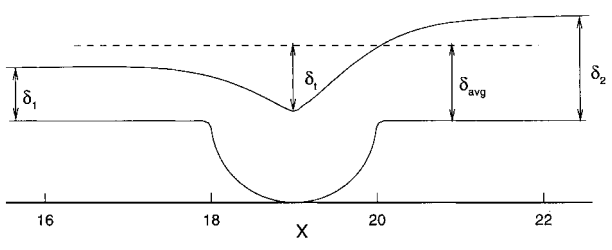

Fig. 8. A schematic illustrating the definitions of δ_t and δ_{avg}.

Figure 10 shows detailed simulation results for $Re = 1$ and $L_a = 0.4$. Clearly, a significant amount of levelling is predicted. The asymmetries in the flux are more significant in this case. Furthermore, the asymmetries persist for longer times; thus, the re-

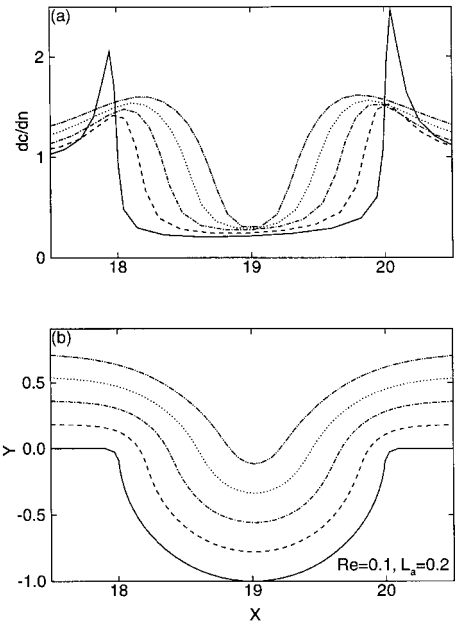

Fig. 9. Evolution of electrode shape and the corresponding flux in the mouth of the trench for $Re = 0.1$ and $L_a = 0.2$. $\delta_{avg} =$ (——) 0, (– – – –) 0.19, (– · – · – ·) 0.37, (……) 0.55 and (– ·· – ·· – ··) 0.73.

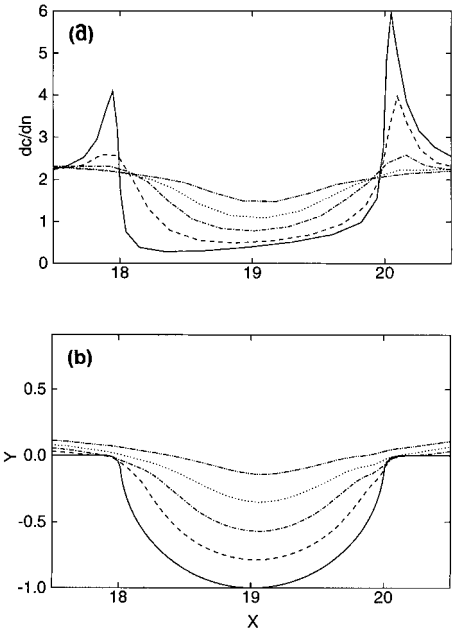

Fig. 10. The evolution of electrode shape and the corresponding flux in the mouth of the trench for $Re = 1.0$ and $L_a = 0.4$. δ_{avg} = (——) 0, (– – – –) 0.04, (– · – · – ·) 0.08, (· · · · · ·) 0.12 and (– ·· – ·· – ··) 0.17.

sulting profile is slightly asymmetric. Nevertheless, the asymmetry is weak even though $Pe = 1000$.

Previous numerical studies use a stagnant diffusion layer approximation to treat the flow. As long as the assumed size of the diffusion layer is very large compared to the scratch dimension, the shape change would only depend on the average levelling power $L_a(\partial c_a/\partial n)\,|_{avg}$. When convective flow is calculated, the shape change should depend on the average levelling power as well as the Reynolds number. Figure 11 shows a comparison of the simulated electrode shape for the same levelling powers, but three different Re. The pure diffusion case is perfectly symmetric as expected. Clearly, the electrode shapes are nearly the same for this case and would probably be indistinguishable experimentally. Figure 12 shows another example for a larger average levelling power. Here differences are much more significant and would probably be seen experimentally.

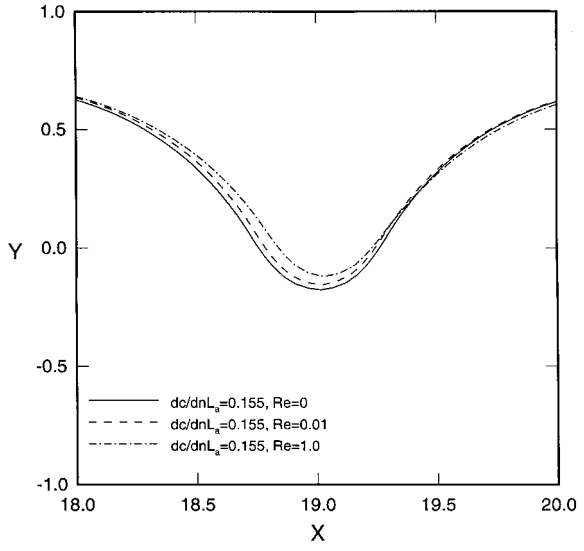

Fig. 11. A comparison of electrode shapes for $Re = 0$ (——), 0.01 (– – – –) and 1.0 (– · – · – ·). In all cases, the same average levelling power is used: $L_a(\partial c_a/\partial n)\,|_{avg} = 0.15$. The profiles are presented for the time at which $\delta_{avg} = 0.72$.

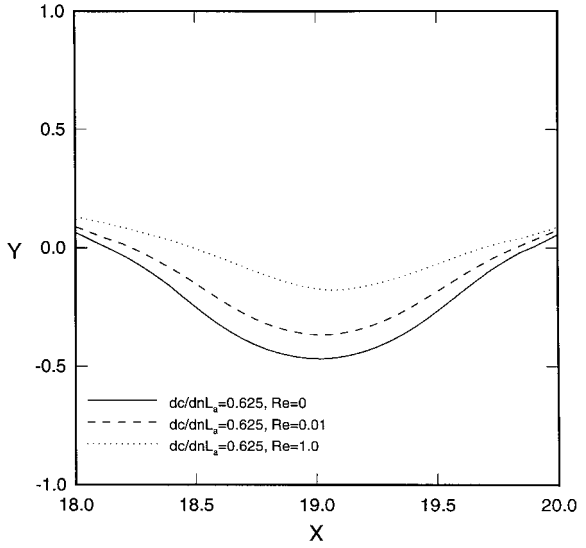

Fig. 12. A comparison of electrode shapes for $Re = 0$ (——) 0.01 (– – – –) and 1.0 (……). In all cases, the same average levelling power is used: $L_a(\partial c_a/\partial n)|_{avg}$ (= 0.62 for $Re = 0$ and 1 and 0.61 for $Re = 0.01$). The profiles are presented for the time at which $\delta_{avg} = 0.25$.

Figure 13 shows a summary of simulation results presented in the same manner as that of Jordan and Tobias [3]. A decrease in δ_t at very high levelling powers in not seen in the present study because the diffusion layer is never sufficiently thin to follow the contour of the scratch. For low average levelling powers, the decrease in δ_t is small, as expected [6, 7]. When the average levelling power increases, significant differences in the curves are apparent. Interestingly, the $Re = 1$ and 0.1 ($Pe = 1000$ and 100) curves lie on top of one another, presumably because both

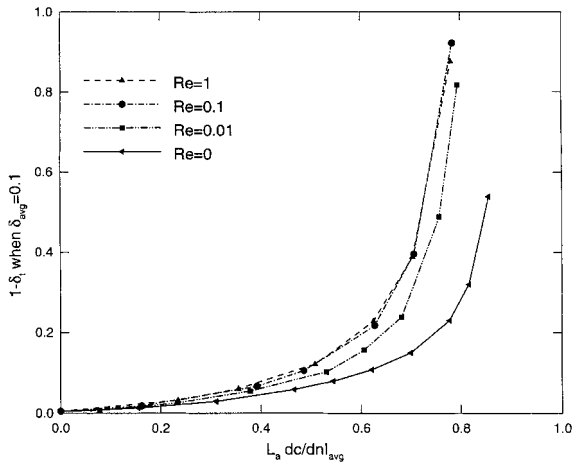

Fig. 13. The dimensionless decrease in trench depth for $\delta_{avg} = 0.1$ as a function of the average levelling power $L_a(\partial c_a/\partial n)\,|_{avg}$ for various Reynolds numbers, Re: (– –▲– –) 1, (– · – ● – · – ·) 0.1, (–·· ■ ··–) 0.01 and (—◀—) 0.

cases correspond to an infinite *Pe* number limit. The $Re = 0.01$ and 0 cases show considerable differences.

For example, for an average levelling power of 0.7, $1 - \delta_t$ varies between 0.15 and 0.39. Such discrepancies are as great as the discrepancies between experiments of Kruglikov *et al*. [4, 5] and the simulations of Jordan and Tobias and Dukovic and Tobias [2, 3]. Likewise, similar discrepancies are found in the study of Madore *et al*. [6, 7]. Apparently, if this plot is the measure of the efficacy of a detailed model for the electrode kinetics (such as Equation 3) in performing levelling studies, a more careful analysis of the fluid flow effects may be required. No attempt is made here to perform such an analysis on the rotating disc measurements of the previous studies, where the flow near the scratch is not easy to analyse. Furthermore, the flow to a disc is impinging instead of a shear flow assumed here. Further work could be improved by performing studies in a flow channel, where the flow can be rigorously analysed.

5. Conclusions

Employment of a stagnant diffusion layer approximation in models of levelling agents may lead to shape changes that qualitatively appear reasonable when compared to more rigorous treatments of flow. However, the ratio of the amount of material deposited at the centre of the 'scratch' to the amount deposited outside the scratch is commonly used as a means of quantitative comparison of simulation and experiment. The present study indicates that such a measure depends on average levelling power as well as the details of the flow fields. The variations due to flow effects can be appreciable, especially for large levelling powers.

Acknowledgement

This work was supported by the National Science Foundation under grant CTS-93-15991.

References

[1] O. Kardos and D. Gardner Foulke, Applications of Mass Transfer Theory: Electrodeposition on Small-Scale Profiles, *in* 'Advances in Electrochemistry and Electrochemical Engineering', Vol. 2 (edited by C. W. Tobias), Interscience Publishers, New York (1962).
[2] J. O. Dukovic and C. W. Tobias, *J. Electrochem. Soc*. **137** (1990) 3748.
[3] K. G. Jordan and C. W. Tobias, *ibid*. **138** (1991) 1251.
[4] S. S. Kruglikov, N. T. Kudriavstev, G. F. Vorobiova and A. Ya. Antonov, *Electrochim. Acta* **10** (1965) 253.
[5] S. S. Kruglikov, N. T. Kudriavstev, A. Y. Antonov and A. V. Dribinski, Proceedings of 6th International Conference on Electrodeposition and Metal Finishing (1965), p.126.
[6] C. Madore, M. Matlosz and D. Landolt, *J. Electrochem. Soc*. **143** (1996) 3927.
[7] C. Madore and D. Landolt, *ibid*. **143** (1996) 3936.
[8] D. Roha and U. Landau, *ibid*. **137** (1990) 824.
[9] C.-C. Chang and A. C. West, *ibid*., **144** (1997) 3050.
[10] K. G. Jordan and C. W. Tobias, *ibid*. **138** (1991) 1933.
[11] P. J. Roache, 'Elliptic Marching Methods and Domain Decomposition', CRC Press, Boca Raton, FL (1995).
[12] P. J. Roache, 'Computational Fluid Dynamics', Hermosa, Albuquerque, NM (1976).
[13] B. F. Armaly, F. Durst, J. C. F. Pereira and B. Schonung, *J. Fluid Mech*. **127** (1983) 473.
[14] H. Cabuk, C.-H. Sung and V. Modi, *AIAA Journal* **30**, (1992) 2024.
[15] J. Newman, 'Electrochemical Systems', 2nd edn, Prentice-Hall, New York (1991).
[16] GridPro/az3000, 'User's Guide and Reference Manual', Program Development Corporation, White Plains, New York (1996).